TECHNICAL REPORT

nature neuroscience

# An *in vivo* biosensor for neurotransmitter release and *in situ* receptor activity

Quoc-Thang Nguyen[1,7], Lee F Schroeder[2,3,7], Marco Mank[4], Arnaud Muller[1], Palmer Taylor[5], Oliver Griesbeck[4] & David Kleinfeld[1,3,6]

**Tools from molecular biology, combined with *in vivo* optical imaging techniques, provide new mechanisms for noninvasively observing brain processes. Current approaches primarily probe cell-based variables, such as cytosolic calcium or membrane potential, but not cell-to-cell signaling. We devised cell-based neurotransmitter fluorescent engineered reporters (CNiFERs) to address this challenge and monitor *in situ* neurotransmitter receptor activation. CNiFERs are cultured cells that are engineered to express a chosen metabotropic receptor, use the $G_q$ protein–coupled receptor cascade to transform receptor activity into a rise in cytosolic [$Ca^{2+}$] and report [$Ca^{2+}$] with a genetically encoded fluorescent $Ca^{2+}$ sensor. The initial realization of CNiFERs detected acetylcholine release via activation of M1 muscarinic receptors. We used chronic implantation of M1-CNiFERs in frontal cortex of the adult rat to elucidate the muscarinic action of the atypical neuroleptics clozapine and olanzapine. We found that these drugs potently inhibited *in situ* muscarinic receptor activity.**



A central tenet of neuronal processing is that unidirectional cell-to-cell communication is based on the release and subsequent binding of cell-signaling molecules. Signaling can be localized to a pair of cells, as occurs with transmission across a synaptic cleft. Signaling can also occur in a volume of tissue through the diffusion of molecules away from the release sites[1,2]. The spillover of glutamate, the excitatory transmitter among central synapses, leads to glutamatergic activation of extrasynaptic metabotropic receptors on nearby neurons and glia. Central modulators, including acetylcholine (ACh), serotonin, norepinephrine and numerous neuropeptides, are commonly released directly into the extracellular space and have long-lasting and long-range effects on central processing. The dual nature of signaling, synaptic versus volume, suggests the possibility of different design strategies for functional probes of these two forms of communications.

The molecular detection of neuronal signaling molecules has been successful in the case of glutamate through the fusion of pairs of fluorescent proteins with bacterial periplasmic proteins that bind small molecules[3–5]. Binding of glutamate leads to a structural change in the periplasmic protein and a subsequent change in fluorescence resonance energy transfer (FRET) between the fluorescent proteins. Conceptually similar work involved the fusion of specific G-protein receptors with pairs of fluorescent proteins[6]. Such functionalized proteins are suitable for the detection of both synaptic and volume transmission. However, each molecular detector must be engineered *de novo* and used in combination with a suitable expression vector. We sought an alternate, modular approach for the detection of neuronal signaling molecules, with a focus on volume signaling.

## RESULTS

Our design exploits the modularity of G-protein receptors and their downstream pathways to expand on concepts from three past technological developments. First, cultured *Xenopus* myocytes that expressed nicotinic ACh receptors have been used as *in vitro* electrophysiological reporters of pulsatile ACh release[7]. This work inspired the development of a cancerous cell line that expressed purinergic receptors for use as a detector of ATP release[8]. Second, high-throughput drug-screening technologies can image receptor-expressing cells, which are loaded with functional fluorescent dyes[9]. Third, implanted cultured cells filled with organic calcium indicators have been used as a test bed for fiber-optic imaging in rat cortex[10]. We expressed G protein–coupled receptors, whose individual subtypes have a high affinity for virtually every known signaling molecule, together with genetically expressible indicators of second messengers to create implantable cellular sensors of receptor activity.

We first used CNiFERs to detect ACh released into the extracellular space[11]. This central modulator has a prominent role in attention, learning and cortical plasticity[12] and is thought to influence the etiology of schizophrenia[13]. M1-CNiFERs were engineered from HEK293 cells by stably expressing the M1 receptor, a major muscarinic receptor in neocortex[14], and the fusion protein and calcium indicator TN-XXL[15] (**Fig. 1a**). Activation of the M1 receptor increased cytosolic calcium in M1-CNiFERs via the $G_q$/inositol triphosphate ($IP_3$) second messenger pathway. The subsequent binding of $Ca^{2+}$ to TN-XXL induces a conformational change that enhances FRET between its cyan and yellow fluorescent protein domains[15]. Thus, M1-CNiFERs report M1 receptor activity by a concurrent decrease in cyan and increase in yellow fluorescence. Lastly, control CNiFERs expressed

[1]Physics Department, [2]Medical Scientist Training Program, [3]Graduate Program in Neurosciences, University of California San Diego, La Jolla, California, USA. [4]Max-Planck Institut für Neurobiologie, Martinsried, Germany. [5]Skaggs School of Pharmacy and Pharmaceutical Sciences, [6]Center for Neural Circuits and Behavior, University of California San Diego, La Jolla, California, USA. [7]These authors contributed equally to this work. Correspondence should be addressed to D.K. (dk@physics.ucsd.edu).

Received 25 August; accepted 17 November; published online 13 December 2009; doi:10.1038/nn.2469

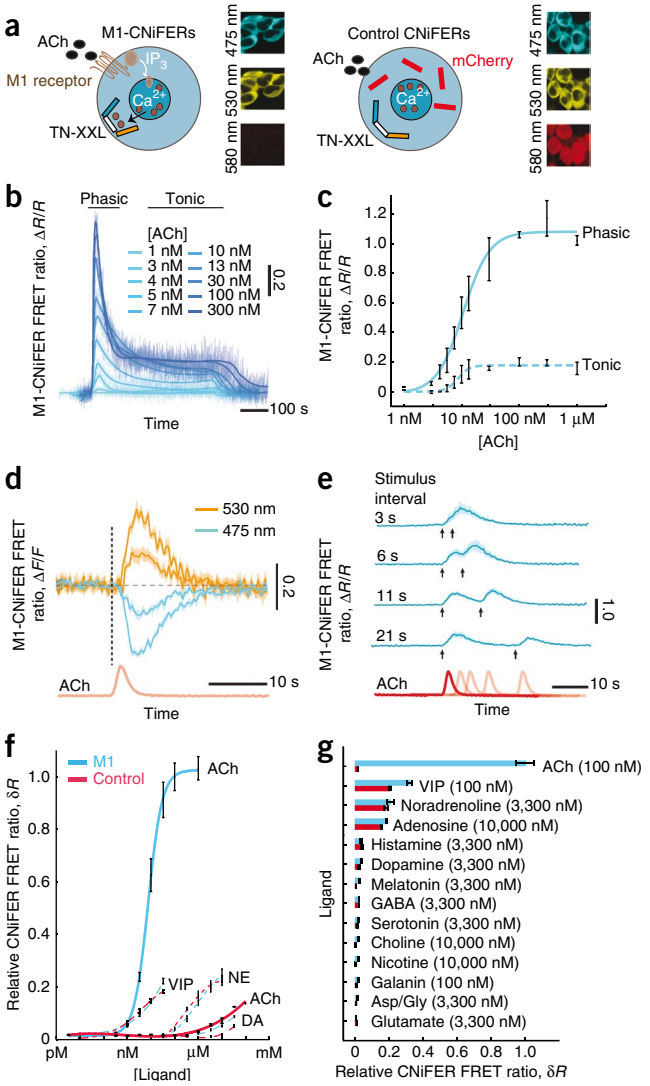


**Figure 1** Design and *in vitro* characterization of CNiFERs. (**a**) CNiFERs were HEK293 cells that stably expressed the M1 muscarinic receptor and TN-XXL (M1-CNiFERs) or TN-XXL and mCherry (control CNiFERs) (Online Methods). In M1-CNiFERs, ACh is depicted as activating M1 to induce $IP_3$-mediated $Ca^{2+}$ cytoplasmic influx detected by TN-XXL. Fluorescence from enhanced cyan fluorescent protein (eCFP) and Citrine cp174 (yellow) fluorescent protein incorporated into TN-XXL were collected for the FRET signal. (**b**) M1-CNiFERs responded to a 500-s bath application of ACh with a phasic response that peaked within ~20–40 s and a tonic plateau that stabilized after ~300 s. (**c**) The M1-CNiFER phasic response to ACh was monotonic in the range of 1–100 nM, with an $EC_{50}$ of 11 nM, a Hill coefficient of 1.9 and a maximum of $\Delta R/R = 1.1$. The tonic response was monotonic in the range of 5–30 nM, with an $EC_{50}$ of 9 nM, a Hill coefficient of 4.4 and a maximum of $\Delta R/R = 0.18$. Phasic responses were measured as the maximum value of $\Delta R/R$ between 0 and 100 s after low-pass filtering of the data at 0.3 Hz, and tonic responses were measured as the average value of $\Delta R/R$ between 300 and 400 s ($n = 3$). (**d**) ACh presentation of ~2.5 s (red trace) to M1-CNiFERs led to opposing responses in cyan (475 nm) versus yellow (530 nm) fluorescence. The response began within 2 s, with a full-width half-maximal response of ~7 s ($n = 5$). (**e**) Two M1-CNiFER FRET-based responses to 100 nM ACh could be discriminated with an interstimulus interval of 6 s or longer ($n = 3$). (**f**) Dose response of M1-CNiFERs (cyan) and control CNiFERs (red) to a subset of endogenous neurotransmitters: ACh, vasoactive intestinal peptide (VIP), norepinephrine (NE) and dopamine (DA) ($n = 5$). (**g**) Summary of screening data at physiologically relevant concentrations. M1-CNiFERs responded with greatest amplitude to ACh, whereas control CNiFERs were nonresponsive to ACh ($n = 3$–5). Error bars represent standard errors.

TN-XXL, but not the M1 receptor; they were distinguished by expression of mCherry fluorescent protein (**Fig. 1a**).

The FRET response of M1-CNiFERs was studied under two-photon laser-scanning microscopy[16] (TPLSM) and the fractional change in FRET was reported as

$$\frac{\Delta R(t)}{R} \equiv \frac{\dfrac{F_{\text{yellow}}(t)}{\left\langle F^{\text{baseline}}_{\text{yellow}} \right\rangle_{\text{prestim}}}}{\dfrac{F_{\text{cyan}}(t)}{\left\langle F^{\text{baseline}}_{\text{cyan}} \right\rangle_{\text{prestim}}}} - 1$$

where background values were subtracted from the individual fluorescence channels and the prestimulus period was typically 10 s. Bath application of a 500-s bolus of ACh (1 to 1,000 nM) revealed two timescales of the M1-CNiFER response. An initial phasic response, with an effective concentration for 10% response level ($EC_{10}$) of 3 nM and an effective concentration for 50% response level ($EC_{50}$) of 11 nM, was followed by a plateau response with an $EC_{10}$ of 5 nM and an $EC_{50}$ of 9 nM (**Fig. 1b**,**c**). These values compare well with the 1–100 nM ACh levels that have been measured in rat brain with microdialysis[17,18]. Lastly, the phasic response was independent of external calcium concentration, whereas the tonic response was abolished in calcium-free media (**Supplementary Fig. 1**).

We further probed the phasic response with a fast perfusion system using 2.5-s applications of 60 or 100 nM ACh, for which the peak changes in relative fluorescence were $\Delta F/F = 0.3$ and 0.9, respectively (**Fig. 1d**). M1-CNiFERs responded within 2 s with a half-maximal rise time of ~2 s and a full width at half-maximal amplitude of ~7 s. We were able to resolve pulses of 100 nM ACh with an interstimulus interval as short as 6 s (**Fig. 1e**). Adaptation of the second response could be seen for the interstimulus interval of 21 s (**Fig. 1e**); further investigation revealed that the peak M1-CNiFER FRET response to pulses of ACh adapted with a time constant of roughly $10^2$ s toward an asymptotic value (**Supplementary Fig. 2**). Lastly, we determined whether M1-CNiFERs respond to a slowly increasing ramp in [ACh] that, in principle, could be undetected if adaptation is strong. For a concentration close to $EC_{50}$, reached over $10^3$ s, sensitivity was maintained (**Supplementary Fig. 3**).

The specificity of M1-CNiFERs was a concern, as HEK293 cells can express endogenous surface receptors. We thus screened for potentially confounding receptor activation on a high-throughput fluorometric plate reader; the atropine-sensitive response of M1-CNIFERs to a saturating level of ACh ([ACh] = 100 nM) served as a reference (**Supplementary Fig. 4**) and we thus report $\delta R^{\text{ligand}}_{\text{M1}} \equiv \Delta R/R|^{\text{ligand}}_{\text{M1}} \big/ \Delta R/R|^{100\,\text{nM ACh}}_{\text{M1}}$ and $\delta R^{\text{ligand}}_{\text{control}} \equiv \Delta R/R|^{\text{ligand}}_{\text{control}} \big/ \Delta R/R|^{100\,\text{nM ACh}}_{\text{M1}}$. First, the activation of control CNiFERs by ACh was negligible; that is, $\delta R^{100\,\text{nM ACh}}_{\text{control}} < 0.05$ (**Fig. 1f**,**g**). Potentially confounding neurotransmitters typically had $EC_{50} > 1$–10 μM and $\delta R^{100\,\text{nM ligand}}_{\text{M1}} < 0.05$ (**Fig. 1g**). Notable exceptions included norepinephrine ($\delta R^{100\,\text{nM NE}}_{\text{M1}} = 0.21$), adenosine ($\delta R^{100\,\text{nM Ad}}_{\text{M1}} = 0.19$) and vasoactive intestinal peptide ($\delta R^{100\,\text{nM VIP}}_{\text{M1}} = 0.33$), which of course activated control CNiFERs (**Fig. 1f**,**g**). M1- and control CNiFERs were implanted in discrete sites in frontal cortex of rat and imaged by

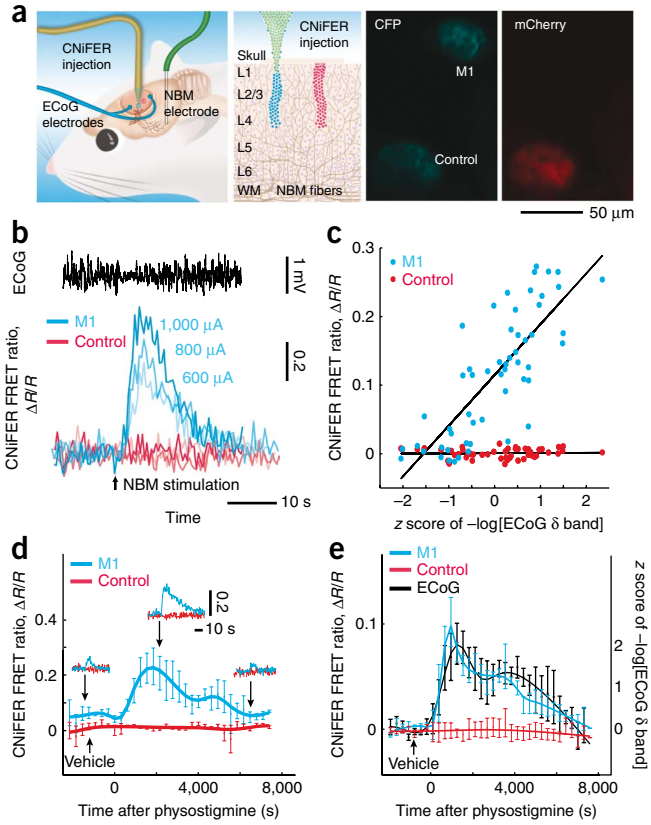


**Figure 2** *In vivo* characterization of acutely implanted M1-CNiFERs. (**a**) Stimulating electrodes were implanted in NBM to recruit the cortical afferent cholinergic system, and ECoG wires were placed to detect NBM-evoked cortical activation (Online Methods). M1-CNiFERs and control CNiFERs were implanted in separate sites in neocortex, whereas cholinergic terminals were widely distributed and imaged acutely or chronically using TPLSM. WM, white matter. Right, two-photon microscopy images of M1-CNiFERs (cyan) and control CNiFERs (red) implanted in rat motor cortex in 25–50-µm diameter columns. Data represent a *z* projection from 40–60 µm below the cortical surface. There are ~10–20 CNiFER cells per site in this field of view. (**b**) M1-CNiFER FRET responses (lower) and ECoG activity (upper) evoked by increasing levels of NBM electrical stimulation. Cortical activation appeared as a shift from large- to small-amplitude waves. Control CNiFERs were nonresponsive. (**c**) The M1-CNiFER response to NBM stimulation was strongly correlated with loss of power in the ECoG δ band, quantified as the *z* score–normalized logarithm of the reciprocal of the power, –log[power in ECoG δ band], for each animal (Online Methods). CNiFER responses were defined as the area under the curve of $\Delta R/R$ for 10 s after the stimulus normalized to that of 10 s before the stimulus ($n = 55$ trials with 4 animals). (**d**) Subcutaneous physostigmine salicylate at 200 µg per kg of body weight enhanced the amplitude and duration of M1-CNiFER responses to NBM stimulation ($n = 3$ animals). The response disappeared by ~8,000 s. Data in bottom trace represent the fractional change of one-third the area under the curve of $\Delta R/R$ for 30 s after the stimulus as compared with that of 10 s before the stimulus. Top traces are examples of raw data used to calculate bottom traces. NBM stimulation occurred every 300 s and phosphate-buffered saline (PBS, vehicle, $n = 3$) was used as a control. (**e**) Subcutaneous physostigmine salicylate at 300 µg per kg caused an increase in baseline M1-CNiFER FRET fluorescence over ~8,000 s ($n = 4$ animals). This is likely to be the result of modulation of background levels of ACh in cortex. M1-CNiFERs (cyan) and control CNiFERs (red) were measured as an average over 10 s every 300 s (top). All measurements were normalized to first three measurements before vehicle injection and not to internal baselines, thus preserving the tonic response. The ECoG data are averaged form four consecutive 5-s epochs for each animal and plotted in black at each time point. Error bars represent standard errors.

TPLSM down to 300 µm below the cortical surface (**Fig. 2**). The typical imaging plane contained contributions from 10–30 CNiFERs per site. We determined whether implanted M1-CNiFERs maintained their functionality by puffing ACh from a pipette inserted near the implantation site. Volume injection of 5–50 nl of 1 mM ACh, but not vehicle, elicited large FRET responses in M1-CNiFERs (**Supplementary Fig. 5**). To determine whether short, physiologically relevant bursts of endogenous ACh will diffuse into the CNiFER sites at detectable concentrations, we electrically stimulated nucleus basalis magnocellularis (NBM), a basal forebrain structure that projects cholinergic fibers into neocortex. Single-train excitation of NBM induced a transient shift in the spectral content of the electrocorticogram (ECoG) that lowered the amplitude of the 1–6 Hz δ-band rhythms for several seconds (**Fig. 2b**) . This ECoG pattern is a hallmark of NBM stimulation[19,20] and was quantified as the *z* score of the negative logarithm of the power in the δ band of the ECoG for a given animal. Concomitantly, M1-CNiFERs responded with a single peak initiated within 2 s, a half-maximal rise time of ~1 s and a width of less than 10 s; simultaneously imaged control CNiFERS did not respond (**Fig. 2b**). This temporal resolution was comparable to that of electrochemistry and ~100-fold faster than microdialysis. Lastly, we observed a strong correlation between ECoG activation and response amplitude in M1-, but not control, CNiFERs ($n = 4$ animals, 55 trials; **Fig. 2c**), an anticipated result[19].

The cholinergic nature of the *in vivo* M1-CNiFER response was verified by subcutaneous injection of physostigmine, an acetylcholinesterase inhibitor, which enhanced the amplitude and duration of the NBM-evoked M1-CNiFER response for ~5,000 s after injection ($n = 3$; **Fig. 2d**). The ability of M1-CNiFERs to detect slow fluctuations in endogenous ACh in the absence of NBM stimulation was tested by administering a relatively high dose of physostigmine to enhance the basal concentration of ACh. We observed a concomitant enhancement in the M1-, but not control, CNiFER FRET ($n = 3$; **Fig. 2e**) that was accompanied by a reduction of power in the δ band of the ECoG. Collectively, these experiments (**Fig. 2**) indicate that CNiFERs can be used to detect small changes in the physiological release of ACh.

Chronically implanted M1-CNiFERs can be imaged for at least 6 d (**Fig. 3a**). Imaging in the *xz* plane showed that the M1-CNiFER response to NBM stimulation extended throughout the depth of the implantation (**Fig. 3a**). The time dependence of the response was very similar to that found with acutely implanted M1-CNiFERs and control CNiFERs remained nonresponsive (11 of 12 rats; **Fig. 3b**). Images of intravenous fluorescein revealed patent vasculature around the implantations (**Supplementary Fig. 6**) and immunohistochemistry demonstrated minimal tissue damage, negligible presence of reactive astrocytes and no evidence for intracortical cell proliferation (**Supplementary Fig. 7**). As confirmation that M1-CNiFERs respond to muscarinic activation, we observed that reverse dialysis of 1–5 µM atropine near the site of implantation acted to reduce the NBM-evoked M1-CNiFER response in a reversible manner ($n = 3$; **Fig. 3c**); a dose of 100 µM atropine essentially abolished the response ($n = 3$; **Fig. 3c**). Pairs of NBM stimuli were resolvable by M1-CNiFERs with an interstimulus interval greater than 5 s (**Fig. 3d**), consistent with *in vitro* experiments (**Fig. 1e**). Finally, the response from chronically recorded M1-CNiFERs was monotonic with increasing stimulation intensity and duration (**Fig. 3e**,**f**), consistent with increased NBM recruitment and augmentation of ACh release in cortex.

To further test M1-CNiFERs, we examined the action of a class of antipsychotic drugs, called atypical neuroleptics[21], on cholinergic

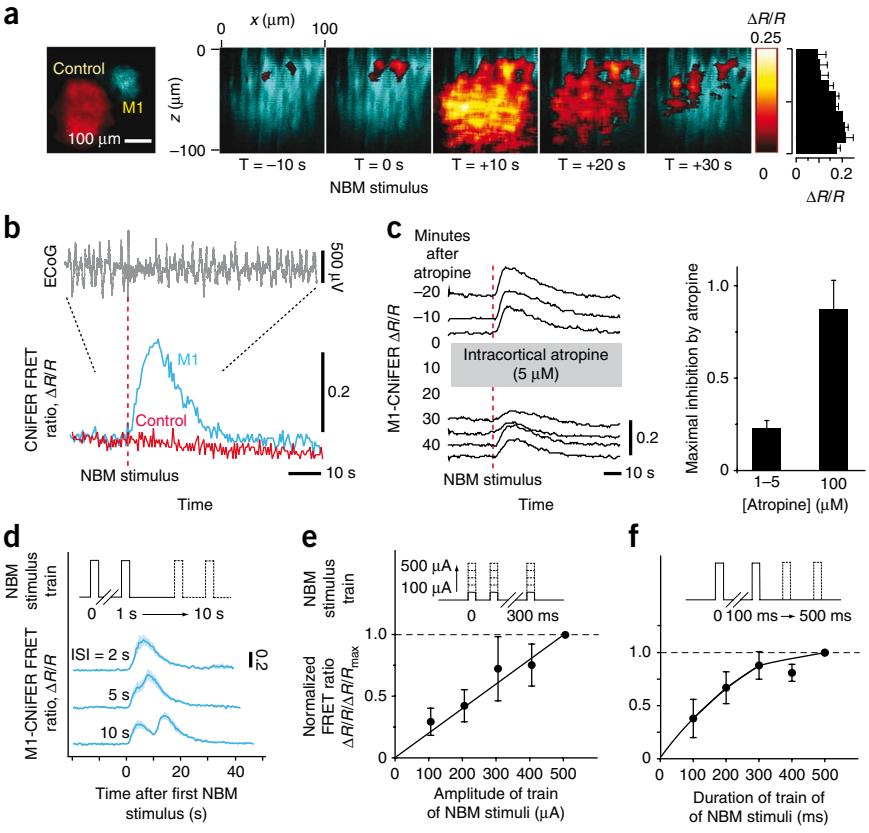


**Figure 3** Chronic implantation of CNiFERs. (**a**) Chronically implanted M1- and control CNiFER sites are shown on the left, an *xz* time series from the M1-CNiFERs in response to a single-train NBM stimulation is shown in the center and the average intensity (mean ± standard error, $n = 4$ animals) of the M1-CNiFER response as a function of depth is shown on the right. (**b**) ECoG and FRET responses in M1- and control CNiFERs in response to NBM stimulation (300-ms train of 300-µA pulses; Online Methods). (**c**) Atropine antagonism. Left, M1-CNiFER responses to single-train NBM stimulation were inhibited by reverse dialysis of intracortical atropine sulfate. Right, average peak inhibition of CNiFER response as a result of the addition of 1–5 µM atropine (23 ± 4%, $n = 4$ rats) or 100 µM atropine (87 ± 16%, $n = 3$ rats). (**d**) Temporal resolution of acutely implanted M1-CNiFERs. Top, stimulation protocol. Bottom, each trace represents the mean response of M1-CNiFERs to two consecutive stimulations of NBM ($n = 5$ for each condition, repeated over 3 animals). (**e**) Response of M1-CNiFERs versus stimulation current. Top, stimulation protocol. Bottom, average M1-CNiFER response normalized to that at 500 µA ($n = 6$ rats). (**f**) Response versus duration of the stimulation train. Top, stimulation protocol. Bottom, average M1-CNiFER response (mean ± s.e.) normalized to that at 500 ms ($n = 6$ rats). The black curves in **e** and **f** are visual aids.



transmission. Atypical neuroleptics, which are used to manage schizophrenia[22], are antidopaminergic compounds with a broad spectrum of activity at other receptors. Many atypicals have marked cholinergic effects that are believed to contribute to their improved therapeutic properties[23]. The atypicals olanzapine and clozapine elicit substantial ACh release peripherally[24] and centrally[25,26], although they are also muscarinic (**Supplementary Fig. 4**)[27,28] and nicotinic antagonists[24]. Furthermore, a bioactive metabolite of clozapine,

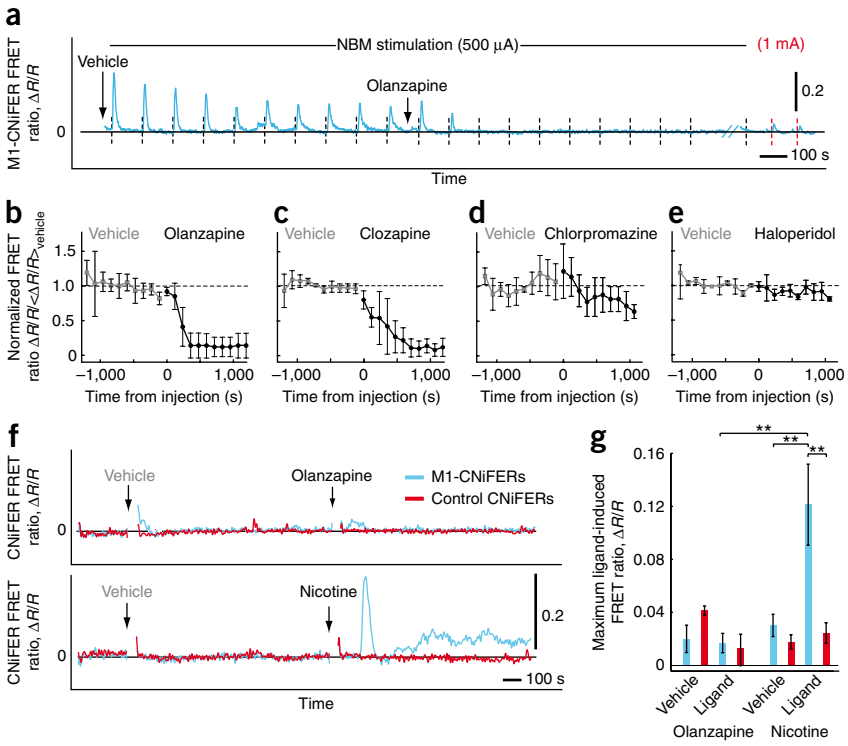


**Figure 4** *In vivo* pharmacology of chronically implanted M1-CNiFERs. (**a**) Olanzapine intraperitoneal injection at 3 mg per kg suppressed the M1-CNiFER response elicited by repetitive NBM stimulation (500 µA, black vertical dashed lines). The M1-CNiFER response was partially recovered by increasing the amplitude of NBM stimulation (1 mA, red vertical dashed lines). (**b**–**e**) Atypical, but not conventional, antipsychotics suppressed the M1-CNiFER response elicited by NBM stimulation. Shown are the M1-CNiFER peak responses normalized to those averaged during vehicle injection, olanzapine at 3–5 mg per kg ($n = 4$), clozapine at 5 mg per kg ($n = 4$), chlorpromazine at 5 mg per kg ($n = 4$) and haloperidol at 1 mg per kg ($n = 3$). (**f**) Olanzapine, injected intraperitoneally at a dose of 10 mg per kg, did not elicit a response in M1-CNiFERs, whereas nicotine ditartrate, injected intraperitoneally at a dose of 0.5–10 mg per kg elicited a response. (**g**) Composite results ($n = 4$ rats) of the maximum response, measured between 120 and 720 s after injection. The response of M1-CNiFERs to nicotine was significantly greater than that for controls, whereas the response of M1-CNiFERS to olanzapine was at chance. $^{**}P < 0.05$, *t* test.

*N*-desmethylclozapine, acts as a muscarinic receptor agonist[29]. Therefore, the net effect of atypicals on muscarinic transmission is controversial[30]. On the one hand, enhanced cholinergic release might explain the effectiveness of atypicals in improving cognition in schizophrenics[29,31]. On the other hand, antagonism of the muscarinic receptor can account for their favorable profile of extrapyramidal side effects[23]. We used M1-CNiFERs to resolve these mutually exclusive alternatives.

We found that the atypical neuroleptic olanzapine profoundly depressed the M1-CNiFER FRET response to periodic stimulation of NBM. In contrast, essentially no change in the FRET response was seen after the injection of vehicle (**Fig. 4a**). The M1-CNiFER response in the presence of olanzapine was partially recovered by an increase in the amplitude of the NBM stimulation (**Fig. 4a**), suggestive of competitive inhibition. The suppressive effects of olanzapine on M1 receptor activation, as well as that of a second atypical neuroleptic, clozapine, were seen across a cohort of animals ($n = 4$ each; **Fig. 4b**,**c**). Clozapine also suppressed NBM-evoked ECoG activation, consistent with a blocking effect on endogenous M1 receptors *in vivo* (olanzapine not tested; **Supplementary Fig. 8**). Further, suppression of M1-CNiFER activation by olanzapine was not dependent on repetitive stimulation, as olanzapine depressed the NBM-evoked response when NBM was first stimulated 1,000 s after the injection of olanzapine (**Supplementary Fig. 9**). As a final control, we found that the conventional antipsychotics chlorpromazine and haloperidol had no observable effect on the NBM-evoked M1-CNiFER response ($n = 3$–4 each; **Fig. 4d**,**e**).

To determine olanzapine's net effect on extrasynaptic muscarinic transmission, as modeled by the response of chronically implanted M1-CNiFERs, we injected olanzapine at a dose known to increase cortical ACh levels sixfold[26]. We found a negligible and statistically insignificant M1-, as well as control, CNiFER FRET response ($P > 0.8$; **Fig. 4f**,**g**). In contrast, nicotine ditartrate, at a dose known to raise cortical ACh levels threefold[32], led to a significant increase in the response of M1-, but not control, CNiFERs ($P < 0.05$; **Fig. 4f**,**g**). Collectively, these results indicate that the atypical neuroleptics clozapine and olanzapine, unlike conventional antipsychotics, are potent *in vivo* inhibitors of extrasynaptic M1 muscarinic receptors as expressed in M1-CNiFERS implanted in frontal cortex. This occurs in spite of their marked ability to stimulate central ACh release[25,26]. Our findings account for the reduced extrapyramidal side effects associated with atypical antipsychotic drugs, as these side effects and antimuscarinic activity are inversely related[33]. They do not support the contention that clozapine and olanzapine activate extrasynaptic cortical M1 receptors indirectly via ACh release.

## DISCUSSION

CNiFERs have high selectivity for a given neurotransmitter (**Fig. 1f**,**g**), but their response adapts on exposure to a constant concentration of agonist. This appeared as a phasic response that decayed to a persistent, tonic level over ~$10^2$ s (**Figs. 1b**,**c** and **4a**). The phasic component did not depend on the external [$Ca^{2+}$] (**Supplementary Fig. 1**) and was consistent with a $Ca^{2+}$ flux derived from the endoplasmic reticulum as part of $IP_3$ receptor activation in the $G_q$-protein cascade[34]. The transition from the larger amplitude of the phasic response to the smaller tonic response can result from a decrement in signaling at any point in the muscarinic $G_q$-protein cascade. Past work implies that there is little desensitization or internalization of the M1 receptor[35]. In contrast, [$Ca^{2+}$] mirrors [$IP_3$] and $IP_3$ signaling exhibits both phasic and tonic components[36], similar to the components that we observed with CNiFERs (**Fig. 1b**). Thus, a rate-limiting step in the generation of $IP_3$, such as the availability of the intermediate phosphatidylinositol 4,5-bisphosphate[37], may explain the adaptation of the CNiFERs. A complementary explanation for the adaptation is that the tonic response is maintained via calcium flux through the cytoplasmic membrane rather than internal calcium stores, as evidenced by the abolishment of the tonic signal in calcium-free media (**Supplementary Fig. 1**).

CNiFERs indirectly report neurotransmitter release, but directly report receptor subtype activity, a measurement that is not possible using microdialysis, electrochemistry or radioisotope tracers. They provide a general approach for observing the *in situ* activation of G protein–coupled receptors by small molecules and peptides in living animals. CNiFERS for $G_q$ protein–coupled receptors, such as those for the molecular transmitters serotonin and prostaglandins, can be engineered as an immediate extension of the M1-CNiFERs and their $Ca^{2+}$-based response. In contrast, CNiFERS for $G_s$ and $G_{i/o}$ protein–coupled receptors, such as those for the peptide transmitters vasoactive intestinal peptide and somatostatin, respectively, can be based on changes in the concentration of cAMP detected via a genetically encoded indicator for the activation of protein kinase A[38]. Alternatively, an endogenous indicator for $Ca^{2+}$ can be used if coexpressed with the promiscuous $G_{\alpha 16}$[39] or $G_\alpha$ chimeras[40]; these G proteins allow receptors not normally linked with the $G_q$ pathway to elicit cytosolic $Ca^{2+}$. Thus, CNiFERs may be used to detect any signaling molecule, of which neurotransmitters are a broad and important class, that activates a G protein–coupled receptor.

## METHODS

Methods and any associated references are available in the online version of the paper at http://www.nature.com/natureneuroscience/.

*Note: Supplementary information is available on the Nature Neuroscience website.*


### ACKNOWLEDGMENTS

We are grateful to T. Bartfai, D.K. Berg, J.-P. Changeux, J.M. Edeline, A.L. Fairhall, B. Hille, H.J. Karten, R. Metherate, P.A. Slesinger, T. Talley, R.Y. Tsien and M. Tuszynski for valuable discussions. We thank R. Figueroa for maintaining the cell culture facility, J. Groisman for preparing the artwork in **Figure 2a** and A. Miyanohara (Vector Development Laboratory, Human Gene Therapy Program, University of California San Diego) for producing the lentiviruses. This work was supported by the US National Institutes of Health Medical Scientist Training Program (L.F.S.), the Max Planck Society (O.G.) and grants from the US National Institutes of Health (DA024206, EB003832 and MH085499 to D.K., GM18360 and DA19372 to P.T., and MH070655 to Q.-T.N.).


### AUTHOR CONTRIBUTIONS

D.K., Q.-T.N. and L.F.S. designed and made the CNiFERs, O.G. and M.M. synthesized the calcium indicator and consulted on molecular biology, D.K., A.M., Q.-T.N., L.F.S. and P.T. characterized and applied the CNiFERS, and D.K., Q.-T.N. and L.F.S. analyzed the data and wrote the manuscript.

### COMPETING INTERESTS STATEMENT

The authors declare competing financial interests: details accompany the full-text HTML version of the paper at http://www.nature.com/natureneuroscience/.


Published online at http://www.nature.com/natureneuroscience/.
Reprints and permissions information is available online at http://www.nature.com/reprintsandpermissions/.



1. Agnati, L.F. *et al.* Volume transmission and wiring transmission from cellular to molecular networks: history and perspectives. *Acta Physiol. (Oxf.)* **187**, 329–344 (2006).
2. Beaudet, A. & Descarries, L. The monoamine innervation of rat cerebral cortex: synaptic and nonsynaptic axon terminals. *Neuroscience* **3**, 851–860 (1978).
3. Tsien, R.Y. Building and breeding molecules to spy on cells and tumors. *FEBS Lett.* **579**, 927–932 (2005).
4. Hires, S.A., Zhu, Y. & Tsien, R.Y. Optical measurement of synaptic glutamate spillover and reuptake by linker optimized glutamate-sensitive fluorescent reporters. *Proc. Natl. Acad. Sci. USA* **105**, 4411–4416 (2008).
5. Okumoto, S. *et al.* Detection of glutamate release from neurons by genetically encoded surface-displayed FRET nanosensors. *Proc. Natl. Acad. Sci. USA* **102**, 8740–8745 (2005).

6. Vilardaga, J.-P., Bünemann, M., Krasel, C., Castro, M. & Lohse, M.J. Measurement of the millisecond activation switch of G protein–coupled receptors in living cells. *Nat. Biotechnol.* **21**, 807–812 (2003).
7. Young, S.H. & Poo, M.M. Spontaneous release of transmitter from growth cones of embryonic neurones. *Nature* **305**, 634–637 (1983).
8. Haas, B. *et al.* Activity-dependent ATP-waves in the mouse neocortex are independent from astrocytic calcium waves. *Cereb. Cortex* **16**, 237–246 (2006).
9. Schroeder, K.S. & Neagle, B. FLIPR: A new instrument for accurate, high throughput optical screening. *J. Biomol. Screen.* **1**, 75–80 (1995).
10. Duff Davis, M. & Schmidt, J.J. *In vivo* spectrometric calcium flux recordings of intrinsic Caudate-Putamen cells and transplanted IMR-32 neuroblastoma cells using miniature fiber optrodes in anesthetized and awake rats and monkeys. *J. Neurosci. Methods* **99**, 9–23 (2000).
11. Umbriaco, D., Watkins, K.C., Descarries, L., Cozzari, C. & Hartman, B.K. Ultrastructural and morphometric features of the acetylcholine innervation in adult rat parietal cortex: an electron microscopic study in serial sections. *J. Comp. Neurol.* **348**, 351–373 (1994).
12. Everitt, B.J. & Robbins, T.W. Central cholinergic systems and cognition. *Annu. Rev. Psychol.* **48**, 649–684 (1997).
13. Raedler, T.J. *et al.* Towards a muscarinic hypothesis of schizophrenia. *Mol. Psychiatry* **12**, 232–246 (2007).
14. Levey, A.I., Kitt, C.A., Simonds, W.F., Price, D.L. & Brann, M.R. Identification and localization of muscarinic acetylcholine receptor proteins in brain with subtype-specific antibodies. *J. Neurosci.* **11**, 3218–3226 (1991).
15. Mank, M. *et al.* A genetically encoded calcium indicator for chronic *in vivo* two-photon imaging. *Nat. Methods* **5**, 805–811 (2008).
16. Denk, W., Strickler, J.H. & Webb, W.W. Two-photon laser scanning fluorescence microscopy. *Science* **248**, 73–76 (1990).
17. Rasmusson, D.D., Clow, K. & Szerb, J.C. Frequency-dependent increase in cortical acetylcholine release evoked by stimulation of the nucleus basalis magnocellularis in the rat. *Brain Res.* **594**, 150–154 (1992).
18. Day, J.C., Kornecook, T.J. & Quirion, R. Application of *in vivo* microdialysis to the study of cholinergic systems. *Methods* **23**, 21–39 (2001).
19. Rasmusson, D.D., Clow, K. & Szerb, J.C. Modification of neocortical acetylcholine release and electroencephalogram desynchronization due to brainstem stimulation by drugs applied to the basal forebrain. *Neuroscience* **60**, 665–677 (1994).
20. Berg, R.W., Friedman, B., Schroeder, L.F. & Kleinfeld, D. Activation of nucleus basalis facilitates cortical control of a brainstem motor program. *J. Neurophysiol.* **94**, 699–711 (2005).
21. Meltzer, H.Y. What's atypical about atypical antipsychotic drugs? *Curr. Opin. Pharmacol.* **4**, 53–57 (2004).
22. Snyder, E.M. & Murphy, M.R. Schizophrenia therapy: beyond atypical antipsychotics. *Nat. Rev. Drug Discov.* **7**, 471–472 (2008).
23. Bymaster, F.P. *et al.* Muscarinic mechanisms of antipsychotic atypicality. *Prog. Neuropsychopharmacol. Biol. Psychiatry* **27**, 1125–1143 (2003).
24. Nguyen, Q.T., Yang, J. & Miledi, R. Effects of atypical antipsychotics on vertebrate neuromuscular transmission. *Neuropharmacology* **42**, 670–676 (2002).
25. Parada, M.A. & Hernandez, L. Selective action of acute systemic clozapine on acetylcholine release in the rat prefrontal cortex by reference to the nucleus accumbens and striatum. *J. Pharmacol. Exp. Ther.* **281**, 582–588 (1997).
26. Ichikawa, J., Dai, J., O'Laughlin, I.A., Fowler, W.L. & Meltzer, H.Y. Atypical, but not typical, antipsychotic drugs increase cortical acetylcholine release without an effect in the nucleus accumbens or striatum. *Neuropsychopharmacology* **26**, 325–339 (2002).
27. Bolden, C., Cusack, B. & Richelson, E. Antagonism by antimuscarinic and neuroleptic compounds at the five cloned human muscarinic cholinergic receptors expressed in Chinese hamster ovary cells. *J. Pharmacol. Exp. Ther.* **260**, 576–580 (1992).
28. Chew, M.L. *et al.* A model of anticholinergic activity of atypical antipsychotic medications. *Schizophr. Res.* **88**, 63–72 (2006).
29. Davies, M.A., Compton-Toth, B.A., Hufeisen, S.J., Meltzer, H.Y. & Roth, B.L. The highly efficacious actions of *N*-desmethylclozapine at muscarinic receptors are unique and not a common property of either typical or atypical antipsychotic drugs: Is M1 agonism a pre-requisite for mimicking clozapine's actions. *Psychopharmacology (Berl.)* **178**, 451–460 (2005).
30. Johnson, D.E. *et al.* The role of muscarinic receptor antagonism in antipsychotic-induced hippocampal acetylcholine release. *Eur. J. Pharmacol.* **506**, 209–219 (2005).
31. Gray, J.A. & Roth, B.L. Molecular targets for treating cognitive dysfunction in schizophrenia. *Schizophr. Bull.* **33**, 1100–1119 (2007).
32. Tani, Y., Saito, K., Imoto, M. & Ohno, T. Pharmacological characterization of nicotinic receptor-mediated acetylcholine release in rat brain: an *in vivo* microdialysis study. *Eur. J. Pharmacol.* **351**, 181–188 (1998).
33. Snyder, S., Greenberg, D. & Yamamura, H.I. Antischizophrenic drugs and brain cholinergic receptors. Affinity for muscarinic sites predicts extrapyramidal effects. *Arch. Gen. Psychiatry* **31**, 58–61 (1974).
34. Krasel, C., Vilardaga, J.P., Bunemann, M. & Lohse, M.J. Kinetics of G protein–coupled receptor signaling and desensitization. *Biochem. Soc. Trans.* **32**, 1029–1031 (2004).
35. Vögler, O. *et al.* Receptor subtype-specific regulation of muscarinic acetylcholine receptor sequestration by dynamin. Distinct sequestration of m2 receptors. *J. Biol. Chem.* **273**, 12155–12160 (1998).
36. Willars, G.B. & Nahorski, S.R. Quantitative comparisons of muscarinic and bradykinin receptor–mediated Ins (1,4,5)P3 accumulation and $Ca^{2+}$ signaling in human neuroblastoma cells. *Br. J. Pharmacol.* **114**, 1133–1142 (1995).
37. Horowitz, L.F. *et al.* Phospholipase C in living cells: Activation, inhibition, $Ca^{2+}$ requirement, and regulation of M current. *J. Gen. Physiol.* **126**, 243–262 (2005).
38. Zhang, J., Hupfeld, C.J., Taylor, S.S., Olefsky, J.M. & Tsien, R.Y. Insulin disrupts beta-adrenergic signaling to protein kinase A in adipocytes. *Nature* **437**, 569–573 (2005).
39. Kostenis, E., Waelbroeck, M. & Milligan, G. Techniques: promiscuous Gα proteins in basic research and drug discovery. *Trends Pharmacol. Sci.* **26**, 595–602 (2005).
40. Coward, P., Chan, S.D., Wada, H.G., Humphries, G.M. & Conklin, B.R. Chimeric G proteins allow a high-throughput signaling assay of Gi-coupled receptors. *Anal. Biochem.* **270**, 242–248 (1999).

## ONLINE METHODS

**Stably expressing cell lines.** CNiFERs were created using replication-deficient lentiviral transduction of HEK293 cells with cDNAs encoding TN-XXL[15], human M1 muscarinic receptor (gift from P. Slesinger, Salk Institute) and mCherry fluorescent protein[41] (gift from R.Y. Tsien, University of California San Diego). M1- and control CNiFERs both expressed TN–XXL, but were differentiated by either M1 receptor or mCherry expression, respectively. cDNAs were subcloned into HIV-based backbone cloning plasmids (System Biosciences). Lentiviral particles were produced by the University of California San Diego Vector Development Laboratory. Serial dilution clonal selection was assisted by puromycin (M1) and fluorescence (TN-XXL and mCherry). CNiFER clones were selected on the basis of their response to ACh and fluorescence intensities. Clones were divided into aliquots and frozen with 10% dimethyl sulfoxide (vol/vol) at $T = -80$ °C. CNiFERs were maintained at 37 °C and 10% $CO_2$ using Fisher Scientific 10 and Forma Scientific 3546 incubators (Thermo Scientific). On confluence (approximately twice weekly), cells were trypsinized, triturated and seeded into new 500-ml flasks with 0.2-μm filtered caps, using Dulbecco's modified Eagle's medium (Cellgro, Mediatech) with addition of Glutamax-1 (Invitrogen) and 10% of Fetalplex serum (vol/vol, Gemini BioProducts). New aliquots of CNiFERs were thawed every 30 to 50 passages.

**TPLSM imaging.** CNiFERs were imaged with a custom two-photon laser-scanning fluorescence microscope[42] that runs the MPScope software suite[43]. A femtosecond laser (Verdi oscillator with Mira pump laser, Coherent) provided excitation light either at 760 nm to visualize mCherry, taking advantage of the anomalous excitation of mCherry at $\lambda < 780$ nm[44] or at 800 nm to excite the eCFP portion of TN-XXL while largely avoiding Citrine cp174. Fluorescence signals, collected by either 20× or 40× water-dipping objectives (UIS2, Olympus), were split into three channels: 455–495 nm (eCFP), 515–545 nm (eCFP and Citrine) and >580 nm (mCherry). *xy* image sizes were 256 × 256 or 512 × 512 pixels taken at 2–3 frames per s. *xz* imaging was achieved in line-scan mode by moving the focal plane with a MIPOS 100 piezoelectric *z*-axis lens positioner (Piezosystem Jena) synchronized with the line scan. *xz* frames sizes were 256 × 256 pixels taken at 2 frames per s.

***In vitro* TPLSM testing.** M1- and control CNiFERs were plated on fibronectin-coated coverslips, placed in a cell-culture chamber (RC26, Warner Instruments) and perfused with artificial cerebral spinal fluid (ACSF: 125 mM NaCl, 5 mM KCl, 10 mM D-glucose, 10 mM HEPES, 3.1 mM $CaCl_2$, 1.3 mM $MgCl_2$, pH 7.4). Chamber fluid temperature was kept at 32 °C by a temperature controller (TC-324B, Warner Instruments). Rapid ACh presentation was achieved with an actuated perfusion stepper (SF-77B, Warner Instruments). The ACh pipette was occasionally coloaded with Alexa-594 to determine actual perfusion times and ACh concentrations. Bath ACh presentation was delivered via gravity feed.

***In vitro* high-throughput testing.** FRET responses of M1- and control CNiFERs to various ligands were measured *in vitro* using a high-throughput fluorometric plate reader (FlexStation 3, Molecular Devices). The day before experiments, M1- or control CNiFERs were seeded onto poly-D-lysine–coated 96-well plates at $0.12 \times 10^6$ cells per well. Media was replaced in each well with 100-μl ACSF and plates were loaded into the FlexStation 3. Experiments were conducted at 37 °C using 435-nm excitation. Emitted light was collected at 485 nm and 527 nm every 3.8 s and ligand was delivered in 50-μl boluses without trituration. Background signals measured from neighboring wells without cells were subtracted, fluorescence intensities were normalized to prestimulus baselines, and peak responses were selected from the ratio of the 527-nm and 485-nm channels. All peaks were then normalized by the M1-CNiFER response to maximal ACh.

***In vivo* surgery and electrode placement.** Adult male Sprague-Dawley rats (250–600 g) were anesthetized with isoflurane according to a standard protocol[45] and implanted with epidural 125-μm Teflon-coated silver-chloride wires across the imaging site for differential ECoG recordings (A-M Systems). In each nucleus basalis magnocellularis (NBM) stimulation experiment, two 0.1 MΩ tungsten stimulating electrodes (Microprobes) spaced ~0.5 mm apart were implanted (coordinates relative to Bregma: 2.1 mm, −1.2 mm, −6.9 mm)[20]. Electrical stimulation consisted of 200-μs current pulses of 100–1,000 μA at 100 Hz for a duration of 20–500 ms. The depth of implantation and the magnitude of current were adjusted to a value that would produce cortical activation, as assayed by reductions in cortical large-amplitude electrical oscillations[46]; this value was typically 200 μA.

***In vivo* implantation.** CNiFERs were triturated from culture flasks without trypsin, concentrated and resuspended in ACSF for injection. After a craniotomy over frontal cortex and dural resection, CNiFERs were loaded into a ~40-μm inner diameter glass pipette connected to a syringe pump and stereotaxically injected ~500 μm from the cortical surface using a syringe pump. Flow was stopped immediately after cells were seen to move down the pipette shaft, and pipette removal was delayed for 5 min to prevent backflow of cells. This procedure expands on the previously described injection of transformed fibroblasts in *ex vivo* gene therapy experiments[47]. After implantation in several adjacent sites, usually 4–5 sites for M1-CNiFERs and 2–3 for control CNiFERs, the craniotomy was filled with 1.5% agarose in ACSF (vol/vol) and sealed with a coverslip using dental cement[48]. Acute and chronic implantations were similar, except that rats were immune-suppressed by daily cyclosporine injection in the latter (Belford Laboratories, 20 μl per 100 g, intraperitoneal) starting 1 d before implantation. For ACh-puffing experiments, an opening into the craniotomy was preserved to allow pipette insertion.

***In vivo* imaging.** All *in vivo* imaging was performed under urethane (1.3–1.5 g per kg, intraperitoneal). For ACh puffing, capillary pipettes with ~25-μm inner diameter were filled with PBS or 1 mM ACh chloride in PBS and affixed to an oocyte injector (Nanoject II). The capillary tip was maneuvered into the window using a micromanipulator (MP-285, Sutter) and positioned near the CNiFER implants. Experimental runs consisted of 10-s baselines followed by 5–50-nl injections. For NBM electrical stimulation experiments, 200-μs pulses of 100–1,000 μA at 20 or 100 Hz were delivered for a duration of 5 s or 20–500 ms, respectively. ECoG signals were amplified with a DAM80 differential amplifier (World Precision Instruments) using a bandpass of 0.1–100 Hz and gain of 1,000. Cerebrovasculature was visualized by injecting 500 μl of 5% fluorescein dextran (wt/vol, Sigma).

***In vivo* pharmacology.** For acetylcholinesterase inhibition experiments, subcutaneous physostigmine salicylate in 100 mM PBS was injected at 200 or 300 μg per kg. Intracerebral atropine perfusion was performed using a syringe pump connected to a microdialysis probe (CMA 11, CMA) implanted 1,000 μm into cortex and ~2 mm from CNiFERs. The flow rate was set to 2 to 15 μl $min^{-1}$. Neuroleptics were dissolved in vehicle using 1% glacial acetic acid in PBS (vol/vol) and a total volume of 1 ml $kg^{-1}$ was injected intraperitoneally. Atypical neuroleptics were used at dosages similar to those in other studies designed to match human therapeutic plasma drug levels[30,49]. Nicotine ditartrate was used for nicotine experiments and delivered at a volume of 1 ml $kg^{-1}$ intraperitoneally. Drugs were purchased from Sigma or AG Scientific.

**Data analysis.** All TN-XXL fluorescence intensities were background subtracted and normalized to prestimulus baselines, as noted in the text, as $\Delta R/R$. *In vitro*, images were averaged to include all cells in the field of view. *In vivo*, regions of interest were drawn around either M1- or control CNiFER implants, generally encompassing 10–150 cells.

For ECoG time series epochs, spectral power densities were estimated using the multitaper algorithm in Chronux Analysis Software for Matlab (http://chronux.org). Poststimulus time series consisted of a single 5-s epoch beginning 600 ms after NBM stimulus onset. Baseline epochs consisted of four, 5-s epochs immediately preceding NBM stimulus onset. We chose a time-bandwidth product of 5 to yield 9 tapers. The measure of δ band ECoG activity was found by calculating the spectral power of each time series, where the time series for the *n*th trial is denoted $V_n(t)$ and the corresponding spectral power is denoted $\tilde{S}_n(f)$, calculating the power in the 1–6-Hz δ band as $\tilde{S}_n^{(\delta)} = \int_{1\text{Hz}}^{6\text{Hz}} df \tilde{S}_n(f)$, taking the logarithm of $\tilde{S}_n^{(\delta)}$, which is $X^2$ distributed, to form the Gaussian distributed variable $\tilde{P}_n^{(\delta)} \equiv -\log_e \tilde{S}_n^{(\delta)}$, where the minus sign reflects the decrease in power with increasing activation, and *z*-score equalizing the log power as $\left(\tilde{P}_n^{(\delta)} - \left\langle \tilde{P}^{(\delta)} \right\rangle\right) \Big/ \sqrt{\left\langle \left(\tilde{P}_n^{(\delta)} - \left\langle \tilde{P}^{(\delta)} \right\rangle\right)^2 \right\rangle}$ to permit comparisons between animals.

Smoothed lines for CNiFER responses were made with the Bayesian adaptive regression splines nonparametric smoothing algorithm for normally distributed data (**Figs. 1b** and **2d**,**e**)[50] (http://www.stat.cmu.edu/~jliebner/).

**Histological procedure.** Adult animals were perfused with PBS for the generation of fresh tissue. The typical perfusion volumes were 0.5 ml per g of body weight and flow rates were 20 ml $min^{-1}$. The PBS perfusion was immediately followed by a second perfusion with 4% paraformaldehyde (wt/vol) in PBS. The extracted brain was stored in 4% paraformaldehyde in PBS for postfixation. Blocking of the tissue, if necessary, was done with a mounted razor blade. Rabbit antibodies to GFAP (Zymed) were used to visualize astrocytes. Sections were quenched in 3% hydrogen peroxide (vol/vol) for 15 min then incubated overnight in a 1:200 dilution of primary antibody to GFAP in PBS containing 0.25% Triton X-100, 5% goat serum and 0.02% sodium azide (wt/vol). After washing for 1 h, sections were incubated in a 1:500 dilution of biotinylated secondary antibody to rabbit (Vector Laboratories). This was followed by the avidin-biotinylated complex method (Vectastain ABC kit, Vector Laboratories) and 3,3′-diaminobenzidine visualization with nickel. Sections were mounted on slides and imaged on an upright microscope with brightfield for 3,3′-diaminobenzidine stains and epifluorescence for M1- and control CNiFERs.


41. Shaner, N.C. *et al.* Improved monomeric red, orange and yellow fluorescent proteins derived from Discosoma sp. red fluorescent protein. *Nat. Biotechnol.* **22**, 1567–1572 (2004).
42. Tsai, P.S. & Kleinfeld, D. *In vivo* two-photon laser-scanning microscopy with concurrent plasma-mediated ablation: principles and hardware realization. in *Methods for In vivo Optical Imaging*, 2nd edn (ed. R.D. Frostig) 59–115 (CRC Press, Boca Raton, 2009).
43. Nguyen, Q.-T., Dolnick, E.M., Driscoll, J. & Kleinfeld, D. MPScope 2.0: A computer system for two-photon laser scanning microscopy with concurrent plasma-mediated ablation and electrophysiology. in *Methods for In vivo Optical Imaging* 2nd edn (ed. R.D. Frostig) 117–142 (CRC Press, Boca Raton, 2009).
44. Drobizhev, M., Tillo, S., Makarov, N.S., Hughes, T.E. & Rebane, A. Absolute two-photon absorption spectra and two-photon brightness of orange and red fluorescent proteins. *J. Phys. Chem. B* **113**, 855–859 (2009).
45. Schaffer, C.B. *et al.* Two-photon imaging of cortical surface microvessels reveals a robust redistribution in blood flow after vascular occlusion. *PLoS Biol.* **4**, e22 (2006).
46. Metherate, R. & Ashe, J.H. Ionic flux contributions to neocortical slow waves and nucleus basalis-mediated activation: whole-cell recordings *in vivo*. *J. Neurosci.* **12**, 5312–5323 (1993).
47. Kawaja, M.D. & Gage, F.H. Morphological and neurochemical features of cultured primary skin fibroblasts of Fischer 344 rats following striatal implantation. *J. Comp. Neurol.* **317**, 102–116 (1992).
48. Nishimura, N. *et al.* Targeted insult to individual subsurface cortical blood vessels using ultrashort laser pulses: three models of stroke. *Nat. Methods* **3**, 99–108 (2006).
49. Shirazi-Southall, S., Rodriguez, D.E. & Nomikos, G.G. Effects of typical and atypical antipsychotics and receptor selective compounds on acetylcholine efflux in the hippocampus of the rat. *Neuropsychopharmacology* **26**, 583–594 (2002).
50. DiMatteo, I., Genovese, C.R. & Kass, R.E. Bayesian curve-fitting with free-knot splines. *Biometrika* **88**, 1055–1071 (2001).